JTTEE5 19:465–475
DOI: 10.1007/s11666-009-9444-9
1059-9630/$19.00 © ASM International

A Study on Arc Instability Phenomena of an Axial Injection Cathode Plasma Torch

P. Mohanty, Jovan Stanisic, Jelena Stanisic, A. George, and Y. Wang

(Submitted April 29, 2009; in revised form September 24, 2009)

Axial injection in plasma gun through the cathode has clear benefit of longer particle residence time and optimum particle trajectory in the plume; however, accelerated wear of the cathode seem to be the major issue in this approach. This study investigates the arc instability phenomena in an axially injecting single cathode plasma torch design. Gun voltage measurements were used to evaluate the arc behavior. For comparison purpose, arc fluctuations with a standard solid cathode torch design under identical operating parameters have also been studied. A comparison of different internal hardware configurations is also done to understand and establish the important factors in the design of the axial injection and solid cathode systems. Further, this study presents the influence of plume elongation and accelerated gas velocities on the arc behavior in different configurations under low pressure environment.

Keywords arc instability, axial injection cathode, low pressure, TaC

1. Introduction

Most conventional plasma spray systems employ radial injection of powders into the plasma stream. Even though temperatures in a plasma plume can exceed 15000 °C, radially injected feedstock does not follow an optimum trajectory within the plasma jet, which reduces the melting fraction of the powder. Further, there are some materials that cannot simply be sprayed because of the short interaction time between the precursor powders and the plume. Therefore, achieving an extended residence time and a uniform trajectory in the plume has been the aim of many design modifications and developments. There have been two main techniques employed to extend this residence time, namely, by means of a low pressure environment to extend the plume or by changing the injection point of the powder.

The benefits of low pressure plasma spray (LPPS) have been realized by the industry for some time now. Many investigations have been carried out on the effects of a low pressure environment on plasma plume elongation. Reports have shown that the plume can be expanded to 10 times (~10^{-4} Pa) its original length in some instances (Ref 1). Although limited, there have been reports on the usefulness of this process even in the case of very hard to spray pure carbides such as tantalum carbide (Ref 2). This approach to extend the particle/plume interaction time is somewhat limited in its flexibility, due to the infrastructure needed to carry out the process. The LPPS process also has other drawbacks. The heat transfer from the plasma jet to the particles is less efficient at low pressure due to Knudsen effect. As a result, finer particles and/or higher enthalpy are required. The deposition rate is low compared to APS process.

In regard to changing the injection point of the powder, the benefits of particle injection point relocation or redirection within or in front of the nozzle have been well documented (Ref 3-14). It has long been realized that axial injection is the best method for increasing the residence time as well as optimizing the particle trajectory. However, axial injection practice in a single cathode configuration is not common. Alternatively, multi-cathode designs have recently appeared in the market to provide the axial injection capability (Ref 4). However, the economics of multi-cathode systems are not as favorable as the common single cathode systems. Multi-cathode systems tend to be bigger and are expensive. Further, the process of changing the worn-out cathode is time consuming compared to single cathode. Often one needs to change all the cathodes to keep uniformity of the arc. Axial injection of particles through a single cathode configuration has been attempted by several researchers (Ref 3, 5, 7, 9-11, 14). Several patents exist based on this concept dating back to 1960s (Ref 15-18). A few studies (Ref 4, 5, 9, 10) have demonstrated that the axial injection plasma spraying is a promising candidate for spraying high melting point materials to form low porosity coatings with

This article is an invited paper selected from presentations at the 2009 International Thermal Spray Conference and has been expanded from the original presentation. It is simultaneously published in *Expanding Thermal Spray Performance to New Markets and Applications: Proceedings of the 2009 International Thermal Spray Conference*, Las Vegas, Nevada, USA, May 4-7, 2009, Basil R. Marple, Margaret M. Hyland, Yuk-Chiu Lau, Chang-Jiu Li, Rogerio S. Lima, and Ghislain Montavon, Ed., ASM International, Materials Park, OH, 2009.

P. Mohanty, Jovan Stanisic, Jelena Stanisic, A. George, and **Y. Wang**, Additive Manufacturing Process Laboratory, University of Michigan, Dearborn, MI. Contact e-mail: pmohanty@umich.edu.

high adhesion. Furthermore, it demonstrates better operating controllability and much more cost effectiveness compared to other plasma spray methods. For example, dense alumina coating was successfully deposited by a 20-kW axial injection plasma spray torch (Ref 14). Even though the need for such a system exists, no commercial vendor has yet introduced a true axial injection system for industrial use.

There seems to be a disconnect between the scientific studies highlighting the merits and the problems of axial injection cathode system. In other words, the number of studies demonstrating the ability to achieve dense and complex coatings of high melting point material at a relatively low power level is much bigger than the number of studies focused on the long-term performance of such a configuration. In fact, the later is limited to a few. Vardelle et al. (Ref 3) were probably the first to conduct a comparative study between classical and axial injection torches by drilling through the cathode. They demonstrated that the axial injection seriously limits the life of the cathode. Further, the operating range of the torch was limited, a too low arc current (<100 amps) resulting in constricted cathode spots and a too high current (>180 amps) inducing a high erosion rate of the cathode. However, other studies have also alluded to the erosion behavior in the passing. For example, Li and Sun (Ref 10) adopted an axial injection cathode made of two tungsten rings, soldered onto a water-cooled rod of copper. The tungsten ring of larger diameter works as the cathode, and the plasma arc root establishes on the surface of ring, while the inner tungsten ring works as a powder injection port. The difference between the front planes of two rings along the axis ensures that the plasma arc originates at the outer tungsten ring. As consequence, the adherence of the powder onto the wall of the cathode can be eliminated through the facile control of particle trajectory and the low temperature of the inner tungsten, resulting from the cooling effect by the powder carrier gas flow. Alternatively, Yugeswaran et al. (Ref 14) have used a single tungsten cap. The cathodic arc strikes between the tungsten cap surface and the anode, while the center hole of the copper cathode acts as a powder injection port. As a consequence, adhesion of spray powder on the cathode wall can be reduced due to the low temperature of the copper wall resulting from the cooling effect by the powder carrier gas flow and forced cathode cooling.

In contrast, electrode erosion phenomenon is a well-studied topic in the conventional single cathode plasma systems. Although much of the earlier developments in torch design to improve the torch stability and electrode wear reduction relied on empirical procedures, recent studies have been devoted to a basic understanding of the arc physics and the plasma jet dynamics (Ref 19-27). In most single cathode/anode DC plasma torches, the arc column is roughly parallel to the anode surface, and a cold gas boundary layer (CBL) electrically insulates the arc column from the anode (Fig. 1a). It is well understood that the arc strikes from the tip region of the cathode to some point on the anode wall where it attaches in the form of a high-temperature, low-density gas column cutting through

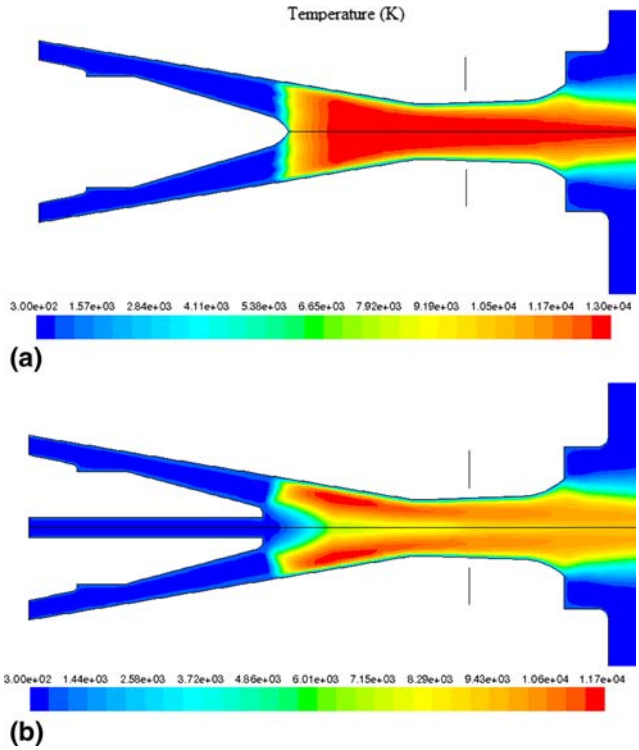

Fig. 1 (a) Predicted temperature profile in a conventional plasma column. (b) Predicted temperature profile in the presence of a centrally injected gas stream (Ar-63.1scfh, He-9scfh, 550 amps)

the CBL that covers the anode wall (Ref 27). While the arc attempts to attach to the anode surface, the drag force exerted by the flow in the boundary layer and the Lorentz forces, try to pull it away. The combined actions of the drag and Lorentz forces make the anode arc attachment to exhibit an axial and rotational movement on the anode surface (Ref 27).

The thickness of the CBL controls the arc behavior and depends on the plasma torch working parameters, namely, the inner column design (of cathode, anode, and exit nozzle), the arc current intensity, and the plasma gas flow dynamics. The symmetry of the anode design favors the rotational movement of the arc. On the contrary, the axial displacement of the arc root brings a variation in the length of the arc column. The electrode life, thermal efficiency, and performance of the plasma devices, are directly or indirectly attributed to the nature of arc fluctuations (Ref 28, 29). As a consequence, the arc behavior in the plasma jet has been the subject of numerous experimental studies. Different arc fluctuation modes have been defined in relation with the thickness of the cold boundary layer: "restrike mode" with a saw-tooth shape profile and high voltage fluctuation, "takeover mode" with a more or less sinusoidal waveform and relative small voltage fluctuation, and "steady mode" with very low mean voltage and voltage fluctuations (Ref 20). The impact of these modes on the electrode life has been explained. Elegant numerical models (Ref 26-28, 30-36) of

the phenomenon have also been developed. To the best of our knowledge, however, the extension of this knowledge and techniques to study the arc behavior in axial injection cathode system is non-existent or at best limited.

Some insight to the arcing phenomena and its relationship to the axial injection cathode design can be made by examining the possible cold boundary layer in this configuration. For this purpose, a simplified fluid flow model was developed utilizing the commercial CFD package FLUENT V. 6.3.26 (ANSYS, Canonsburg, PA) to simulate the plasma flow field. On the basis of a generally accepted assumption, the plasma flow was considered to be optically thin, chemically inert, and in local thermodynamic equilibrium (LTE). A simple approach was adopted to simulate the complicated arc phenomena, where a volumetric energy source was introduced inside the torch nozzle to account for the Joule heating effect of the arc on the plasma-forming gas (Ref 37). Hence the electromagnetic phenomena, such as the electrodes losses, and Lorenz force, were not considered in this study. This method provides simplistic projections of the flow fields by using the electric power as the sole input data. Further simplifications include:

- The plasma flow was assumed to be steady, not taking into account the energy fluctuation caused by the arc root movement.
- As no magneto-hydrodynamic effect was included in this model, the swirl introduction of the gas around the cathode is not taken into account.
- The radiation loss was neglected, since the mean temperature in the column is not very high (~12000 K).

The mass, momentum, and energy conservation equations, along with the species transport equations, were solved using the finite-volume approach for a two-dimensional axis-symmetric domain. Pressure-velocity coupling was achieved by the SIMPLEC algorithm. The Reynolds-Stress model (RSM) is utilized to model the turbulence in the plasma flow. A mixture of Ar/He is supplied through the plasma gas injector. In the axial injection cathode models, Ar is also introduced through the center hole of the cathode as the carrier (cooling) gas while keeping the total gas flow constant between the two models. The anode wall and cathode wall are maintained at a constant temperature of 1000 K. The plasma jet is discharged into open atmosphere (100 kPa) or into the low-pressure chamber (6 kPa).

The thermodynamic and transport properties of the plasma gases and air are taken from the study of Boulos et al. (Ref 38), the properties of the gas mixtures are then calculated using the semi-empirical formula proposed by Wilke (Ref 39) and Mason (Ref 40).The properties and mixing laws were incorporated into Fluent code through a number of user-defined functions. The parameters used in these simulations were the same as the conditions under which measurements were carried out in this study (described below). The temperature profiles of a conventional plasma column as well as an equivalent axial

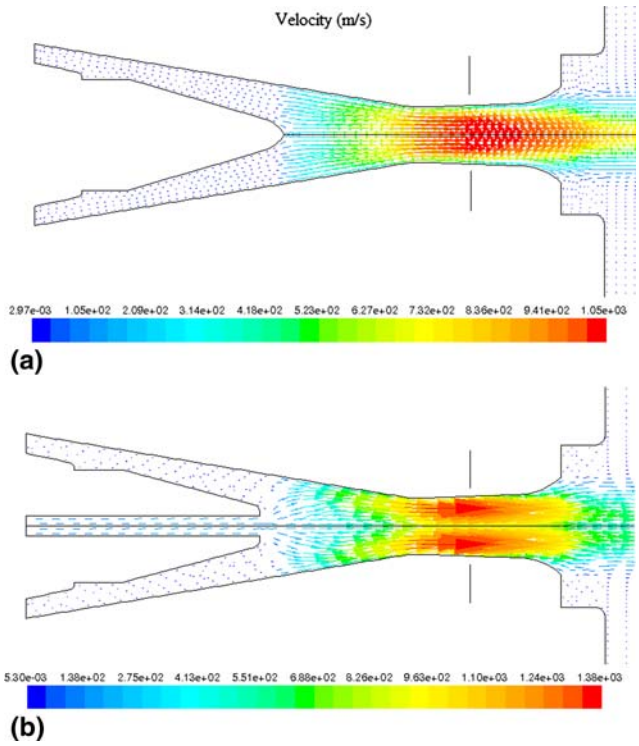

Fig. 2 (a) Predicted velocity profile in a conventional plasma column. (b) Predicted velocity profile in the presence of a centrally injected gas stream

injection cathode plasma column are shown in Fig. 1. The corresponding velocity profiles are shown in Fig. 2.

As seen from Fig. 1(b), the axial injection cathode system has a central cold zone due to the injection of the carrier gas. Accordingly, the velocity profile (Fig. 2b) is also significantly altered. Even if the plasma jet is constricted farther downstream by the anode nozzle, the influence of the central cold gas stream on the temperature as well as the velocity profile is still considerable. From these simulations, it is reasonable to assume that the arc emanates from the ring of the cathode forming a hollow cylindrical plasma jet. This is because, in the presence of the central gas stream, it will be difficult for the arc root to attach on the internal surface of the cathode. In fact, a study (Ref 7) on the voltage-ampere measurement does show that when the central gas is absent, the gun voltage jumps up indicating arc root attachment inside the cathode. This so called ''hollow arc,'' however, would necessitate that either the arc root moves randomly or its rotation overlays the whole ring-shaped end of the cathode for stable torch operation.

As mentioned earlier, the plasma jet experiences rotational as well as axial movement. Owing to the presence of a hollow core, the rotational movement may not be affected significantly; however, the axial movement is expected to be influenced. Utilizing the techniques and tools employed to study the conventional plasma arc, this study intends to gain insight to the behavior of the hollow arc. Further, in order to study the influence of plume

elongation, the arc voltage measurements were also performed in a LPPS environment. The primarily focus here is to examine the effects of the internal geometry and the environment on the arc fluctuation behavior to further the understanding of the axial injection cathode system.

2. Experimental Procedure and Details

Axial injection single cathode systems are not commercially available. Therefore, new hardware was designed and manufactured to enable axial injection. In nutshell, the design could also accommodate the standard cathode, anode, and gas injector used in Praxair SG100 plasma torch (Danbury, CT). The measurements were carried out utilizing the newly designed axial injection cathode configuration and the standard SG-100 configuration as the reference. The gun was powered by a Thermach (Appleton, WI) 60-kW power supply and control panel. Internal hardware of the standard system consisted of a subsonic cathode (Praxair #2083-720), subsonic anode (Praxair #2083-730), and a 4-hole gas injector (Praxair #2083-113). The axial injection cathode system consisted of cathode, anode, and gas injector designed by the University of Michigan A.M.P.L. laboratory, and hereafter referred to as UM-cat, UM-ano, and UM-inj, respectively. All the experiments were conducted utilizing new hardware to avoid any preferential arc root attachment spot. The environment was controlled within a range of 6-9.33 kPa (~0.03 atm) for all the LPPS experiments. For the APS experiments, the chamber was vented in; however, the pressure was slightly higher (~106.6 kPa) than the atmosphere (101.325 kPa). The plasma torch was operated with argon as the primary gas, and helium as the secondary gas. Gas mass flow rate was held constant in all the experiments, with argon and helium at 51.185 slpm (4.45 kg/h), and 4.522 slpm (0.045 kg/h), respectively. The operating parameters and the hardware configurations are shown in Table 1. The axial injection cathode design has a constant argon gas flow through the center to cool the cathode as well as feed the powder during operation. In order to equalize the mass flow rate between the two designs, additional primary gas was used for the standard design to compensate for the lack of the central gas injection. Most of the experiments intended to find what effects, if any, are attributed to the changes in internal geometry alone, and therefore were conducted with no powder injection (see Table 1). The second set of experiment intended to study the effects of powder injection on the stability of the axial injection cathode design. These tests were conducted utilizing the P1V hardware setup, and are identified as tests P2V, P3V, and P4V (see Table 1). Both the metallic alloy and the ceramic powders were injected separately, and simultaneously. The ceramic powder was injected axially, while the metallic was injected through the standard radial powder port location of the SG100 plasma torch.

The data acquisition setup consisted of a PC (personal computer), a NI SCXI 1000 4-slot chassis, SCXI 1600 USB

Table 1 Operating parameters and hardware configurations

Pressure, kPa	Hardware Anode-cathode-gas injector	Amp	Test name
6.132	UM-ano, UM-cat, UM-inj	550	P1V
101.325	UM-ano, UM-cat, UM-inj	550	P1
6.132	P1V, with Ceramic powder	550	P2V
6.532	P1V, with Ceramic/Metallic powder	550	P3V
6.932	P1V, with Metallic powder	550	P4V
7.332	2083-730, 2083-720, 2083-113	550	P5V1
101.325	2083-730, 2083-720, 2083-113	550	P5
7.466	2083-730, UM-cat, 2083-113	550	P6V
101.325	2083-730, UM-cat, 2083-113	550	P6
6.799	UM-ano, UM-cat, 2083-113	550	P7V
101.325	UM-ano, UM-cat, 2083-113	550	P7
9.199	2083-730, UM-cat, UM-inj	550	P8V
101.325	2083-730, UM-cat, UM-inj	550	P8
7.332	UM-ano, 2083-720, UM-inj	550	P9V
101.325	UM-ano, 2083-720, UM-inj	550	P9
7.332	2083-730, 2083-720, UM-inj	550	P10V
101.325	2083-730, 2083-720, UM-inj	550	P10
7.332	UM-ano, 2083-720, 2083-113	550	P11V
101.325	UM-ano, 2083-720, 2083-113	550	P11

Data Acquisition (DAQ) Module, two SCXI 1120 devices with two high voltage attenuator blocks of SCXI 1327 (National Instruments, Austin, TX). The device was configured for an input of 0-10 V, and the gun anode and cathode terminals were connected to the DAQ device through a voltage transducer, CV 3-500 (300 kHz bandwidth) which converts the gun voltage to a voltage of 0-10 V. Care was taken to ensure that the sampling rate of the setup was capable of measurements up to 200 kHz frequency, and the sampling rate was set at 200 kS/s to satisfy the Nyquist criterion. The data were stored in the PC for offline analysis in LabView (National Instruments, Austin, TX). Voltage fluctuations were sampled at the plasma torch to eliminate any resistive effects of the power cable. Measurements were taken only after the prescribed environmental pressure was established and held constant for a minimum of 1 min in an effort to minimize pressure fluctuation. Each experiment was sampled for 5 s yielding a data set of 1 million points. Sections were independently analyzed in 200 k point sets.

3. Results and Discussion

The data were analyzed in the time domain as well as in the spectral domain by means of FFT computation. The FFT was taken by subtracting the mean from the data and also by low pass filtering of the data so that the frequency components, characteristic of the gun operation can be extracted. Some useful information such as average voltage, $\bar{u}$ and the standard deviation, u_{sd} was obtained from the time domain data. The calculations for $\bar{u}$ and u_{sd} are defined as followed.

$$\bar{u} = \frac{1}{N}\sum_{i=1}^{N} u_i \qquad \text{(Eq 1)}$$

$$u_{sd} = \sqrt{\frac{1}{N-1}\sum_{i=1}^{N}(u_i - \bar{u})^2} \quad \text{(Eq 2)}$$

Different arc fluctuation modes have been defined in relation to the thickness of the cold boundary layer (Ref 20). Accordingly, certain figures of merit, which give an insight into the gun operation modes, were established. These include the amp factor (A) and shape factors (Sh). The shape factor Sh by definition is:

$$\text{Sh} = \frac{t_{up}}{t_{down}} = \frac{\text{number of instances where } u_{i+1} > u_i}{\text{number of instances where } u_{i+1} < u_i} \quad \text{(Eq 3)}$$

where t_{up} and t_{down} denote the time duration of the upward slope and the downward slope, respectively. The underlying theory to this ratio is that in the restrike mode, the voltage ramps up relatively slowly followed by a steep decline. During takeover mode, these times are relatively equal. This leads to a fundamental characteristic that the restrike mode has a high Sh factor, and the ideal takeover mode has a Sh value of 1. While the steady mode has a flat voltage trace resulting in a low $\bar{u}$ and u_{sd}. The steady mode has been linked to the accelerated anode wear. An amp factor A was also introduced by Ref 20, but modified by Vysohlid (Ref 41) as a better method for measuring an irregular signal. The amp factor was calculated by means of the average voltage $\bar{u}$, standard deviation u_{sd}, and is defined as follows:

$$A = \frac{u_{sd}}{\bar{u}} \times 100\% \quad \text{(Eq 4)}$$

It has been previously established (Ref 20) that a perfect restrike mode exists when $A \geq 10$, and Sh ≥ 5. A prefect takeover mode exists when $A \geq 10$, and Sh < 1.1. The steady mode was defined as $A < 2$, while a takeover-steady mixed mode was $2 < A < 10$, and the restrike-takeover mixed mode was $A \geq 10$, and Sh < 5.

On the basis of the above guidelines, all the voltage data were analyzed in our experiments. An average shape factor and average amp factor were calculated for all the experiments listed in Table 1. The results are shown in Fig. 3. For all the cases investigated here (Table 1), the condition of $2 < A < 10$ was observed indicating that the gun ran in a takeover-steady mixed mode. The shape factor for all the experiments met the condition, Sh < 1.1. In other words, the axial injection cathode design operated in a steady/takeover mixed mode, such as the standard SG100 subsonic configuration. Further, under the LPPS condition investigated here (~6 kPa), the arc mode did not change from the APS conditions. As mentioned earlier, the arc behavior is influenced by the boundary layer that is established on the anode wall. The decrease in operating pressure of the chamber from 106.6 to 6 kPa is expected to have influence on the flow field. Therefore, it is reasonable to expect that it should influence the flow field inside the gun and in turn the arc mode. Although, there were differences in the amp factor between APS and LPPS experiments (the latter being slightly higher in most cases), the magnitude was not significant to indicate any change in the arc mode.

Figure 4 compares the voltage traces for the axial injection cathode configuration under the APS and LPPS environments. Although the mean voltages for both the cases are almost the same, there is a slight difference in the standard deviation. Figure 5 presents the comparison of voltage traces for the conventional cathode configuration under APS and LPPS environments. Compared with the case of the axial injection cathode, the mean voltage as well as the standard deviation in Fig. 5 differed appreciably between the APS and LPPS measurements. The APS mean voltage was higher whereas the LPPS standard deviation was higher. In general, the standard deviation of arc voltage fluctuations goes up when the boundary layer is thicker. As discussed above, the transition from APS to LPPS may affect the boundary layer and, in turn, the arc behavior. Also note that the standard gun is operated at a higher voltage than the axial injection cathode gun, which is related to the larger arc root area.

On the basis of the shape factor and amp factor, the axial injection cathode and the solid cathode systems seem to run under steady/takeover mixed mode. Also note that the corresponding FFTs for the two systems under LPPS condition are very similar as shown in Fig. 6. No dominant peak frequencies were present for both the cases except the ones attributed to the power supply. However, a closer examination of the voltage traces (Fig. 7) between the axial injection cathode and the solid cathode configuration under LPPS environment reveals some interesting features.

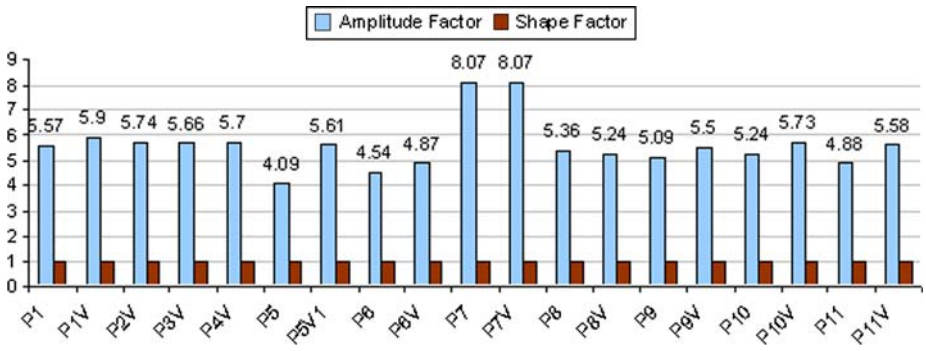

Fig. 3 Shape factor and amp factor results for the experimental matrix in Table 1

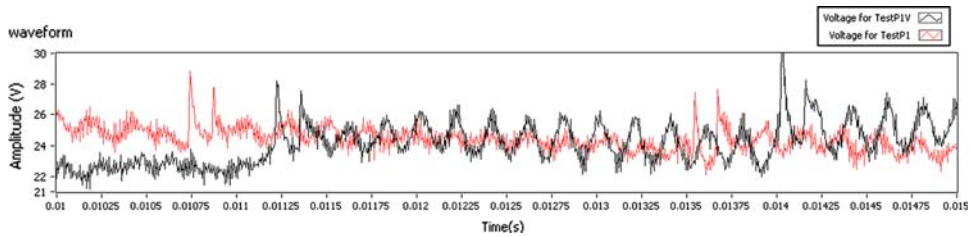

Fig. 4 Axial injection cathode voltage, P1 (red, $\bar{u} = 24.33$ V, $u_{sd} = 1.36$ V) and P1V (black, $\bar{u} = 24.35$ V, $u_{sd} = 1.41$ V)

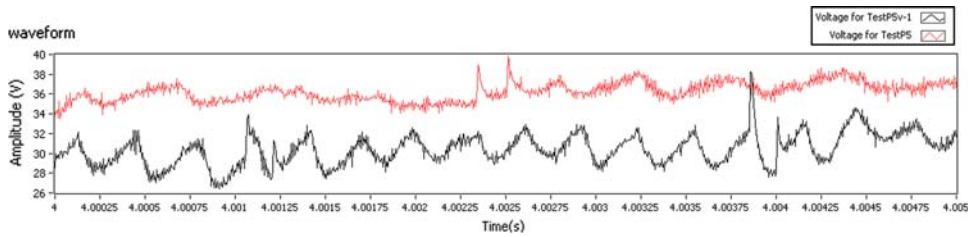

Fig. 5 Standard SG100 voltage, P5 (red, $\bar{u} = 35.8$ V, $u_{sd} = 1.48$ V) and P5V1 (black, $\bar{u} = 30.18$ V, $u_{sd} = 2.29$ V)

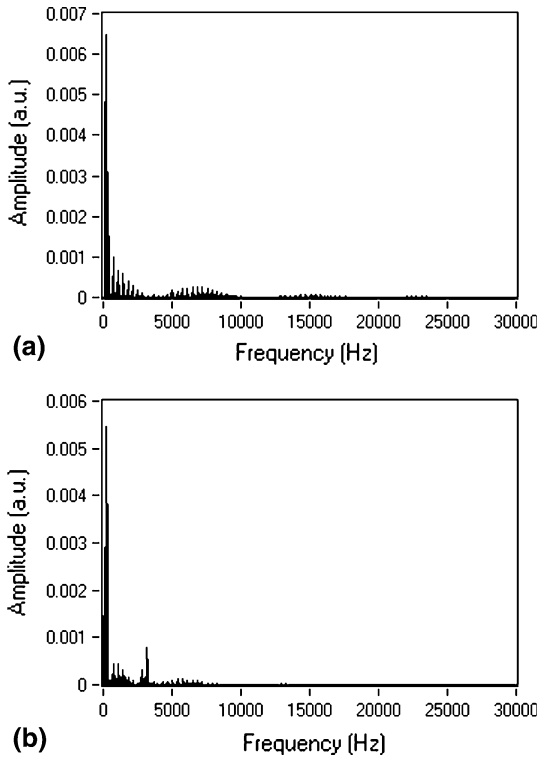

Fig. 6 FFTs of voltage signal; (a) axial injection (P1V) cathode and (b) solid (P5V1) cathode

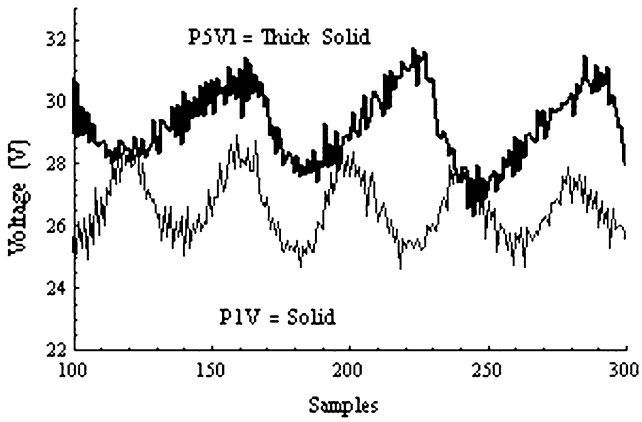

Fig. 7 Voltage signal; solid (P5V1), and axial injection (P1V) cathode

For the axial injection cathode, the voltage trace has a sinusoidal wave form indicating a takeover mode. On the contrary, for the case of the solid cathode, a restrike (slow voltage ramps up followed by a rapid decline) character is apparent. It is to be noted that based on the shape factor and amp factor, the voltage data presented in Fig. 7 are still considered to be takeover-steady mixed mode. However, the solid cathode configuration has more restrike characteristics in the voltage trace.

Further insight into this difference discussed above can be made by examining the simulated velocity and temperature fields for both the systems under LPPS environment presented in Fig. 8 and 9. As expected, the plumes have expanded considerably farther outside the throat of the nozzle. Closer examination also reveals that for the axial injection cathode system the velocity gradient as well as the temperature gradient (Fig. 10) across the throat of the anode is shallower, compared to the case of the solid cathode system. Therefore, the observation of a restrike character (with higher standard deviation) in the case of solid cathode under LPPS (higher velocity) condition is reasonable. Plume length variation under LPPS condition in the case of conventional plasma system has been

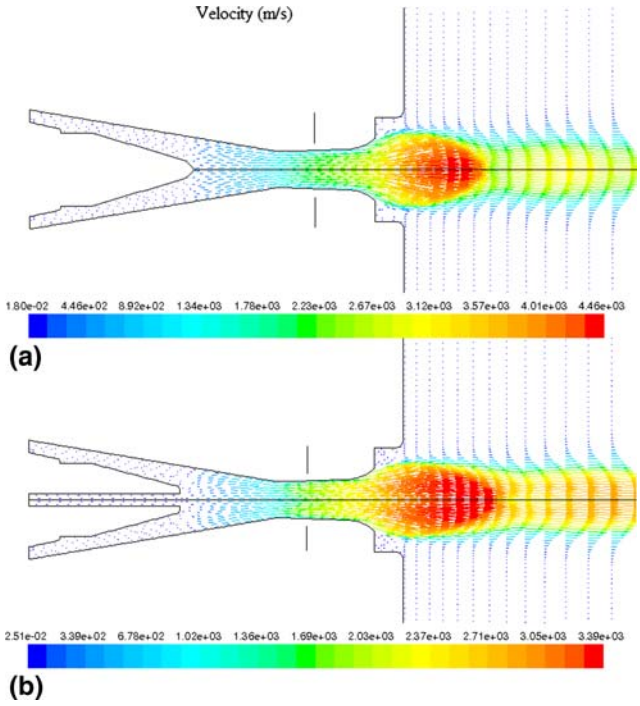

Fig. 8 (a) Velocity profile in LPPS (6 kPa) environment, conventional torch, (b) axial injection cathode (Ar-63.1scfh, He-9scfh, 550 amps)

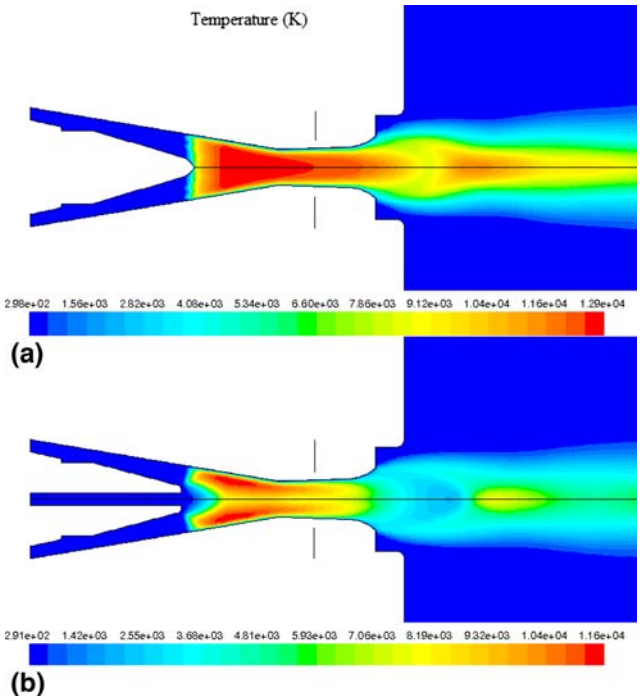

Fig. 9 (a) Temperature profile in LPPS (6 kPa) environment; conventional torch, (b) axial injection cathode (Ar-63.1scfh, He-9scfh, 550 amps)

measured with high speed imaging technique by Kieschke et al. (Ref 42). An obvious inference from the observed periodicity of the fluctuations was that they were induced

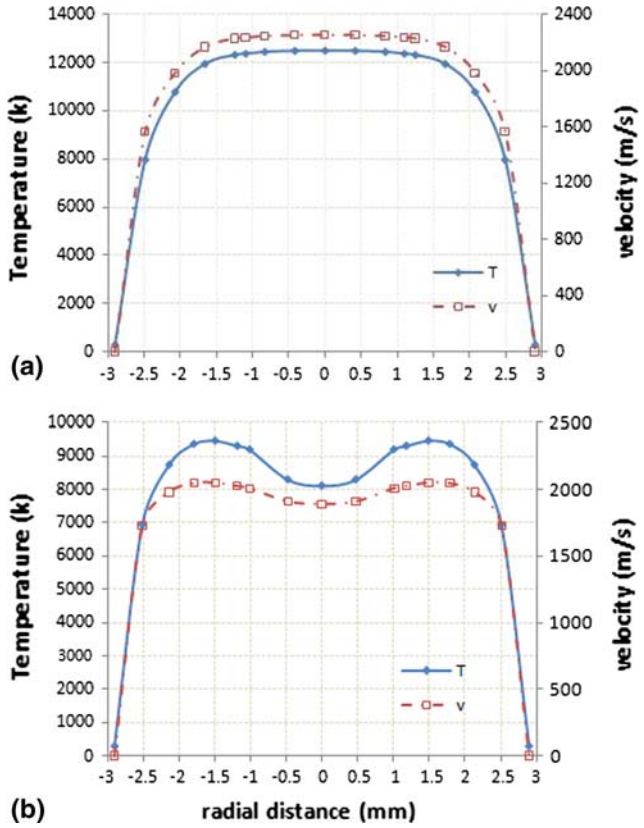

Fig. 10 (a) Cross-section temperature-velocity profile for solid cathode (from Fig. 8a and 9a). (b) Cross-sectional temperature-velocity profile for solid cathode (from Fig. 8b and 9b)

by a ripple in the electrical transformer, particularly as 300 Hz is a common ripple frequency from a three-phase full-wave rectified system. However, the fluctuations associated with the arc restrike phenomenon were not observed, possibly due to the low frame rates used in their experiments. From the voltage signal as well as simulation results, it appears that the central gas from the axial injection cathode configuration affects the arc behavior appreciably under LPPS condition compared to that of the APS environment.

Figures 11 and 12 present the comparison of the voltage signals as affected by the gas injector. Our injector design (Fig. 13) differs from the standard SG100 (#2083-113) 4-hole design. As seen from these signals, the gas injector influenced the $\bar{u}$ considerably for the axial injection cathode system whereas the u_{sd} was not affected as much. Figure 3 clearly shows the difference in P7 and P7V from all other combinations. Our injector design showed a jump in the mean voltage, indicating that the arc root moved more randomly or its rotation overlaid the whole ring of the cathode. Alternatively, a diffused attachment of the arc at the whole tip of the cathode is also possible (Ref 3). The latter would limit the operational range of the gun: too low a current would result in a constricted arc root, and too high a current would induce high erosion rate of the cathode. For the applications in our study, we

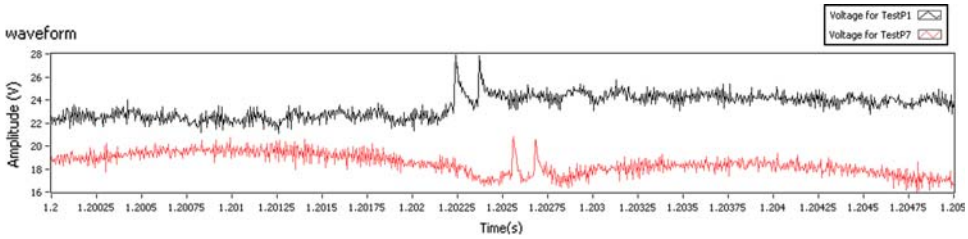

Fig. 11 Voltage trace, P1 (black, UM injector, $\bar{u} = 24.33$ V, $u_{sd} = 1.36$ V) and P7 (red, 4 hole injector, $\bar{u} = 18.9$ V, $u_{sd} = 1.5$ V)

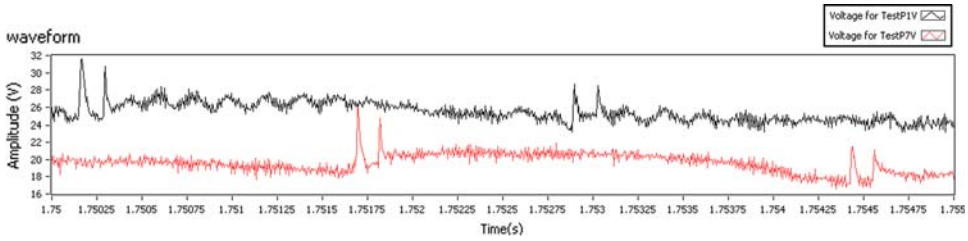

Fig. 12 Voltage trace, P1V (black, UM injector, $\bar{u} = 24.35$ V, $u_{sd} = 1.41$ V) and P7V (red, 4 hole injector, $\bar{u} = 18.19$ V, $u_{sd} = 1.44$ V)

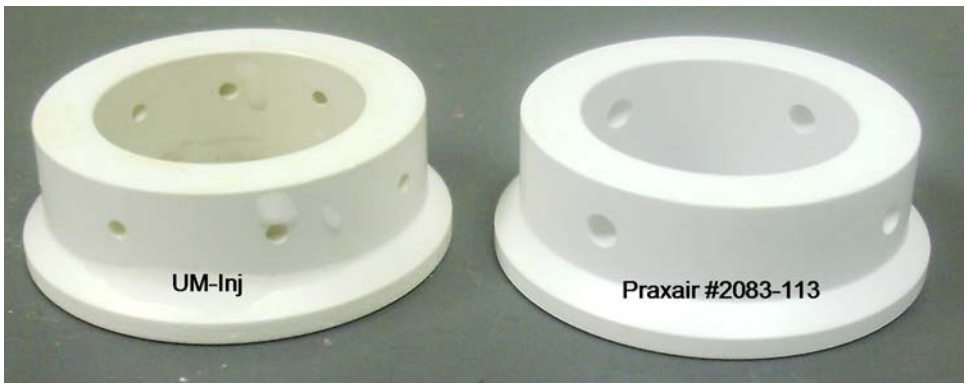

Fig. 13 (a) UM injector, (b) Praxair #2083-113

did not need high power, and, therefore, cannot validate the erosion behavior at higher power. However, there have been reports of gun operating up to 300 kW (Ref 11). The LPPS environment did not influence the gas injector effect as shown in Fig. 12. The standard 4-hole injector induced more fluctuations in the arc as evident from high amp factor, accelerating the deposition of powders on anode wall as will be discussed later.

The next point of interest is to evaluate what effect, if any, particle injection has on the arc fluctuation. It is possible that electrically nonconductive particles injected into the path of the arc might influence the attachment and reattachment behavior and, consequently, induce erratic voltage fluctuations. First, a stream of ceramic particles was injected through the axial injection cathode only. The voltage measurements were then recorded as P2V. Then a metallic powder was injected at the standard anode injection point together with coaxial ceramic particle injection. The measurements were recorded as P3V. In the third measurement, the metallic powder was injected only at the standard anode injection point. This point of injection is located after the usual arc attachment points and normally does not have much of an effect on stability, but was included for completeness. This test was annotated as P4V. The shape factor analysis exhibits little-to-no effect caused by the powder injection, as shown in Fig. 3.

By definition, tests P1V-P4V exhibit a steady/takeover mixed mode operation with little change in their shape and amp factors. Similarly, a global inspection of the voltage measurements of these tests shows no apparent change in the waveform with similar $\bar{u}$ and u_{sd} afters the powder is introduced into the axial injection cathode (Fig. 14). However, a closer examination (Fig. 15) shows that the signal has become noisy after the introduction of the powder into the cathode, although the overall nature of the waveform remains intact. The P1V and P4V tests exhibit the same type of waveform, where the P2V and P3V

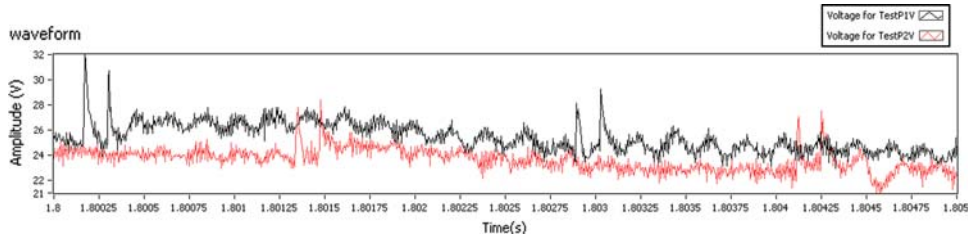

Fig. 14 Axial injection cathode voltage, P1V (black, $\bar{u} = 24.35$ V, $u_{sd} = 1.41$ V) and P2V (red, $\bar{u} = 24.39$ V, $u_{sd} = 1.4$ V)

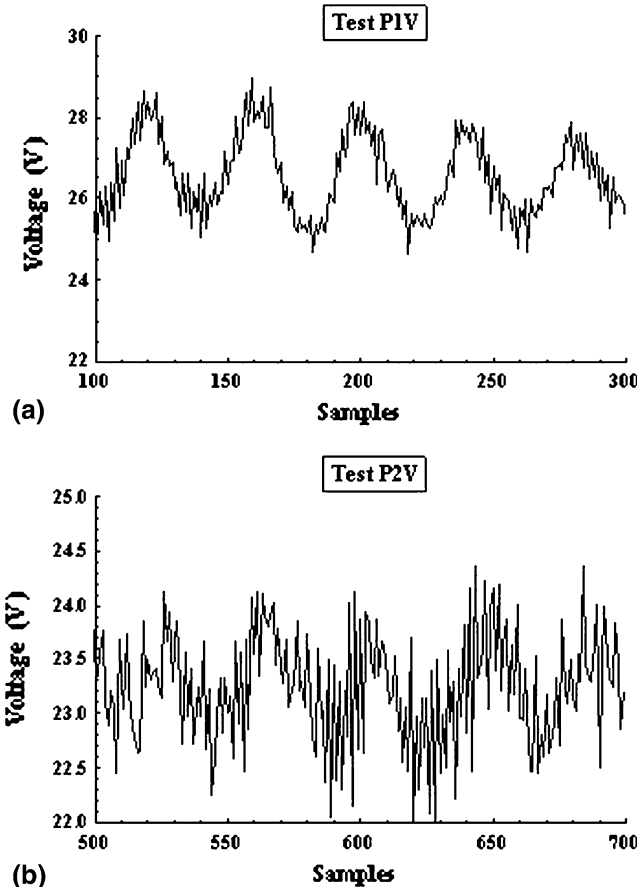

Fig. 15 Axial injection cathode voltage, P1V (top, $\bar{u} = 24.35$ V, $u_{sd} = 1.41$ V) and P2V (bottom, $\bar{u} = 24.39$ V, $u_{sd} = 1.4$ V)

tests show spiking as shown on the lower plot of Fig. 15. From these observations, it appears that powder introduction into the axial injection cathode somehow influences the cathode spot of the arc. As mentioned earlier, in the presence of the central gas stream, it will be difficult for the arc root to attach on the internal surface of the axial injection cathode, and a study (Ref 7) does show that when the central gas is absent, the gun voltage jumps up indicating arc root attachment inside the cathode. This scenario is not expected to change when the central gas carries powder with it. On the other hand, the particle injection with a carrier gas through the cathode may present the same problems as those observed with standard plasma torches i.e., a dispersion of the particle trajectories, and it is unavoidable to have particles passing at the periphery of the hollow arc column. However, studies (Ref 3) performed on the injection of particles in transferred arcs have shown that the natural tendency of the arc is to find its path aside the particle flow. Therefore, the plausible cause for noise spikes may be due to the erosion of the hot cathode by the injected particles.

From the above discussion, it is evident that the axial injection cathode gun design operates mainly in the steady/takeover mixed mode of operation. Pure restrike mode was not exhibited in the range of this study, regardless of hardware configuration. It should be mentioned that most Ar/He plasma guns operate in the range where the takeover mode dominates. Under LPPS environment, the axial injection cathode design also showed takeover mode dominance. This takeover mode has been a proven operating mode for the production of good coatings. However, experiments with the axial injection cathode design under APS environment often led to operational difficulties. Axial injection under APS environment resulted in particles being redirected from their original flight trajectory and consequently adhered to the anode wall eventually causing clogging of the anode. When spraying a ceramic, a noticeable drop in operating voltage occurs during this time of build-up, and/or clogging. It is believed that the voltage drop is caused by the non-conductive properties of the ceramic forcing the arc to attach at a point closer upstream on the anode instead of further downstream in the nozzle area of the anode. As discussed above, the operational (electrical characteristics) modes of the axial injection cathode design under APS and LPPS environment are not significantly different, and, therefore, the observed particle clogging behavior does not seem to be related to the electrical behavior. However, a comparison of the velocity fields (Fig. 2b and 8b) of the axial injection cathode design under APS and LPPS environments, suggests a different reason. For the APS case (Fig. 2b), the velocity vectors point toward the anode wall in the immediate vicinity of the cathode tip. Dispersion of particles toward the anode wall will be favorable under this circumstance. On the contrary, from Fig. 8(b), it is evident that the velocity vectors align along the anode axis in cathode tip region and, therefore, the particle trajectories are expected to follow the axis.

While LPPS condition favors desired particle trajectory, the temperature field may have some adverse effect. The simulated temperature (Fig. 9b) field under LPPS

Table 2 Typical properties of Cr_2O_3 and TaC

Material	Melting temp, °C	Thermal conductivity, W/m K	Gun design type	Power, kW
Chromium oxide (Cr_2O_3)	2490	10-34	SG100 standard subsonic	40.5
Tantalum carbide (TaC)	3880	22.1	New	17.6

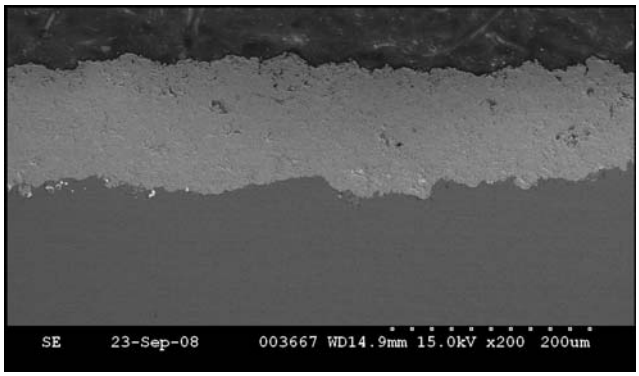

Fig. 16 APS tantalum carbide coating

condition suggests that the axial injection cathode design does not provide any special advantage in terms of the length of the hot zone in the jet. In fact, the high temperature zone is smaller than the one that existed in the APS condition (Fig. 1b). It should be noted that the whole notion of LPPS plasma spraying is to benefit from the extended plume and higher particle velocity. The advantage of LPPS operation for standard gun is quite evident from Fig. 9(a). The axial injection cathode design itself provides the opportunity of extended interaction. In order to prevent oxidation, one can operate the gun under inert environment instead of LPPS environment. Alternatively, one can optimize the LPPS condition to achieve the desired particle trajectory and an optimized temperature field.

It is to be noted that most of the experiments were conducted at a much lower power level (~15-20 kW) compared with many conventional plasma guns. Even at this lower power level, the extended residence time in the hot zone of the plasma plume enables one to spray a wide variety high temperature material. For example, Table 2 shows the physical properties of chromium oxide (Cr_2O_3), a widely used plasma-spraying material. The not-so-common or not so easily sprayable tantalum carbide (TaC) properties are also included in this table. It is worth noting that the power consumption in the axial injection design for spraying TaC is less than half of that is commonly used for spraying Cr_2O_3 by the standard gun despite their melting points being significantly different (Table 2). In order to demonstrate the capability of this new design, the micrograph of a TaC deposit is shown in Fig. 16. This coating was obtained in atmospheric condition at power level indicated in Table 2. Note that success with plasma spraying of TaC is limited, and that to LPPS (Ref 2). As shown here, a good coating was feasible at a very low operating power by the axial injection cathode design.

4. Conclusion

The arc behavior of an axial injection single cathode plasma gun was investigated in this study. The characteristic mode of the arc for the axial injection cathode design was observed to be in the steady/takeover mixed mode. The arc behavior did not change significantly from APS to LPPS environment. The gas injector design influenced the mean voltage considerably for the axial injection cathode system whereas the standard deviation was not affected as much. Increasing the number of holes while keeping the overall cross section area constant showed a jump in the mean voltage, indicating that the arc root moved more randomly or its rotation overlaid the whole ring of the cathode. Particle introduction also did not affect the overall arc behavior. However, the signal became noisy after the introduction of the powder into the cathode, although the overall nature of the waveform remained intact. The plausible cause for noise spikes is believed to be due to the erosion of the hot cathode by the injected particles. Axial injection under APS environment resulted in particles being redirected from their original flight trajectory and consequently adhered to the anode wall eventually causing clogging of the anode. When spraying a ceramic, a noticeable drop in operating voltage occurs during this time of build-up and/or clogging. Flow field modification under LPPS environment suppressed this problem. However, the melting efficiency was lowered, which was in line with the predicted temperature profile. An optimized LPPS condition to achieve the desired particle trajectory and temperature field performed well. This new design is capable of producing coatings that previously were not possible with comparable conventional plasma guns. The overall power consumption in this design was low.

Acknowledgments

Financial support from the US Navy under Contract No: N00244-07-P-0553 is gratefully acknowledged. The authors are also thankful to Mr. Tim VandenHeuval, and Thermach Inc, for their close collaboration and support.

References

1. W. Ma, W.X. Pan, and C.K. Wu, Preliminary Investigations on Low-Pressure Laminar Plasma Spray Processing, *Surf. Coat. Technol.*, 2005, **191**, p 166-174
2. K. Balani, G. Gonzalez, A. Agarwal, R. Hickman, J.S. O'Dell, and S. Seal, Synthesis, Microstructural Characterization, and Mechanical Property Evaluation of Vacuum Plasma Sprayed Tantalum Carbide, *J. Am. Ceram. Soc.*, 2006, **89**(4), p 1419-1425
3. M. Vardelle, A. Vardelle, and P. Fauchais, Comparison of Classical and Axial Injection Torches for Spraying Alumina Coatings, *Mater Manuf. Proc.*, 1994, **9**(4), p 735-755

4. L.C. Erickson, T. Troczynski, H.M. Hawthorne, H. Tai, and D. Ross, Alumina Coatings by Plasma Spraying of Monosize Sapphire Particles, *J. Therm. Spray Technol.*, 1999, **8**(3), p 420-426
5. S. Sharafat, A. Kobayashi, S. Chen, and N. Ghoniem, Production of High-Density Ni-Bonded Tungsten Carbide Coatings Using an Axially Fed DC-Plasmatron, *J. Surf. Coat. Technol.*, 2000, **130**, p 164-172
6. M. Vardelle, A. Vardelle, P. Fauchais, K.I. Li, B. Dussoubs, and N.J. Themelis, Controlling Particle Injection in Plasma Spraying, *J. Therm. Spray Technol.*, 2001, **10**(2), p 267-284
7. L. Lie, W. Beyi, and W. Cheng-kang, Characteristics of Plasma Spraying Torch with a Hollow Cathode, *Plasma Sci. Technol.*, 2001, **3**(2), p 749-754
8. K. Brinkiene, R. Kezelis, L. Pranevicius, D. Milcius, A. Baltusnikas, and V. Mecius, Role of Particle Injection Characteristics on Coating Microstructure of Plasma Sprayed Zirconia, *Mater. Sci.*, 2003, **9**(1), p 35-39
9. C. Li and B. Sun, Microstructure and Property of Al_2O_3 Coating Microplasma-Sprayed Using a Novel Hollow Cathode Torch, *Mater. Lett.*, 2003, **58**, p 179-183
10. C. Li and B. Sun, Effects of Spray Parameters on the Microstructure and Property of Al_2O_3 Coatings Sprayed by a Low Power Plasma Torch with a Novel Hollow Cathode, *Thin Solid Films*, 2004, **450**, p 282-289
11. S. Sharafat, A. Kobayashi, and N. Ghoniem, Application of High-Power Plasma Gun for Thermal Cycle Testing of Refractory Foams, *Vacuum*, 2004, **73**, p 475-480
12. V. Srinivasan, M. Friis, A. Vaidya, T. Streibl, and S. Sampath, Particle Injection in Direct Current Air Plasma Spray: Salient Observations and Optimization Strategies, *Plasma Chem. Plasma Process.*, 2007, **27**, p 609-623
13. L. An, Y. Gao, and T. Zhang, Effect of Powder Injection Location on Ceramic Coatings Properties When Using Plasma Spray, *J. Therm. Spray Technol.*, 2007, **16**(5-6), p 967-973
14. S. Yugeswaran, V. Selvarajan, D. Seo, and K. Ogawa, Effect of Critical Plasma Spray Parameter on Properties of Hollow Cathode Plasma Sprayed Alumina Coatings, *J. Surf. Coat. Technol.*, 2008, **203**, p 129-136
15. G.M. Giannini and C. Ducati, Plasma Stream Apparatus and Methods, Plasmadyne Corp. US United States Patent 2,922,869, 26 January 1960
16. D. Whyman, Plasma Arc Device with Cathode Structure Comprising Plurality of Rods, U.S. Patent 3,433,991, 18 March 1969
17. M. VardelIe, P. Fauchais, and I. Saray, Injection Par Cathode, ANVAR Patent No. 19541, 1 October 1981; ANVAR Patent 19545, 1989
18. I. Zaplatynsky, Plasma Gun with Coaxial Powder Feed and Adjustable Cathode, U.S. Patent No. 4990739, 5 Feb 1991
19. J. Hlina and V. Nénicka, Identification of Local Oscillations in a Plasma Jet, *Prog. Plasma Process. Mater.,* 1999, p 333-337
20. Z. Duan and J. Heberlein, Arc Instabilities in a Plasma Spray Torch, *J. Therm. Spray Technol.*, 2002, **11**, p 44-51
21. C. Chazelas, J.F. Coudert, and P. Fauchais, Arc Root Behavior in Plasma Spray Torch, *IEEE Trans. Plasma Sci.*, 2005, **33**(2), p 414-420
22. J. Dorier, M. Gindrat, C. Hollenstein, A. Salito, M. Loch, and G. Barbezat, Time-Resolved Imaging of Anodic Arc Root Behavior During Fluctuations of a DC Plasma Spraying Torch, *IEEE Trans. Plasma Sci.*, 2001, **29**(3), p 494-501
23. J.F. Bisson, B. Gautier, and C. Moreau, Effect of Plasma Fluctuations on in-Flight Particle, *J. Therm. Spray Technol.*, 2003, **12**, p 38-43
24. L. Leblanc and C. Moreau, The Long-Term Stability of Plasma Spraying, *J. Therm. Spray. Technol.*, 2002, **11**(3), p 380-386
25. S. Janisson, A. Vardelle, J.F. Coudert, E. Meillot, B. Pateyron, and P. Fauchais, Plasma Spraying Using Ar-He-H_2 Gas Mixtures, *J. Therm. Spray. Technol.*, 1999, **8**(4), p 545-552
26. R. Hartmann and J. Heberlein, Quantitative Investigations on Arc-Anode Attachments in Transferred Arcs, *J. Phys. D Appl. Phys.*, 2001, **34**(19), p 2972-2978
27. E. Meillot, D. Guenadou, and C. Bourgeois, Three-Dimension and Transient D.C. Plasma Flow Modeling, *Plasma Chem. Plasma Process.*, 2008, **28**(1), p 69-84
28. E. Moreau, C. Chazelas, G. Mariaux, and A. Vardelle, Modeling the Restrike Mode Operation of a DC Plasma Spray Torch, *J. Therm. Spray. Technol.*, 2006, **15**(4), p 524-530
29. P. Fauchais, Understanding Plasma Spraying, *J. Phys. D: Appl. Phys.*, 2004, **37**, p R86-R108
30. J.P. Trelles, E. Pfender, and J. Heberlein, Thermal Nonequilibrium Simulation of an Arc Plasma Jet, *IEEE Trans. Plasma Sci.*, 2008, **36**(4), p 1026-1027
31. E. Meillot and D. Guenadou, Thermal Plasma Flow Modeling: A Simple Model for Gas Heating and Acceleration, *Plasma Chem. Plasma Process.*, 2004, **24**(2), p 217-238
32. E. Meillot and G. Balmigere, Plasma Spraying Modeling: Particle Injection in a Time-Fluctuating Plasma Jet, *Surf. Coat. Technol.*, 2008, **202**(18), p 4465-4469
33. H.P. Li and E. Pfender, Three Dimensional 3D Simulation of a DC Transferred Arc Plasma Modeling of the Plasma Spray Process, *J. Therm. Spray Technol.*, 2007, **16**(2), p 245-260
34. J.P. Trelles and J. Heberlein, Simulation Results of Arc Behavior in Different Plasma Spray Torches, *J. Therm. Spray Technol.*, 2006, **15**(4), p 563-569
35. J.P. Trelles, E. Pfender, and J. Heberlein, Multi Scale Element Modeling of Arc Dynamics in a D.C. Plasma Torch, *Plasma Chem. Plasma Process.*, 2006, **26**, p 557-575
36. J.P. Trelles, J. Heberlein, and E. Pfender, Non-Equilibrium Modelling of Arc plasma Torches, *J. Phys. D Appl. Phys.*, 2007, **40**, p 5937-5952
37. G. Mariaux and A. Vardelle, 3-D Time-Dependent Modelling of the Plasma Spray Process. Part 1: Flow Modeling, *Int. J. Therm. Sci.*, 2005, **44**, p 357-366
38. M.I. Boulos, P. Fauchais, and E. Pfender, *Thermal Plasmas: Fundamentals and Applications*, Vol 1, Plenum Press, 1994
39. C.R. Wilke, A Viscosity Equation for Gas Mixtures, *J. Chem. Phys.*, 1950, **18**(4), p 517
40. E.A. Mason and S.C. Saxena, Approximate Formula for the Thermal conductivity of Gas Mixtures, *Phys. Fluids*, 1958, **1**(5), p 361
41. M. Vysohlid and J. Heberlein, Investigation of Arc Voltage Fluctuations in a Plasma Torch SG-100 Operated with Ar/H_2, *Proceedings of the International Thermal Spray Conference*, May 10-12, 2004 (Osaka, Japan), ASM International, 2004, p 998-1003
42. R.R. Kieschke, K.A. Roberts, and T.W. Clyne, Instabilities in the Vacuum Plasma Spraying Process, *J. Surf. Coat. Technol.*, 1991, **46**, p 25-38